Surface second-harmonic generation enhanced by an ultrahigh-Q microresonator

Xueyue Zhang[1,2], Qi-Tao Cao[1], Yu-xi Liu[2,3], Qihuang Gong[1], Yun-Feng Xiao[1]

June 13, 2017

Second-order nonlinear optical processes lie in the heart of many applications in both classical and quantum regime, e.g. frequency conversion, quantum squeezing and entanglement. Inversion symmetry inhibits the second-order nonlinear dipole response in plenty of materials widely used in integrated photonics such as SiO_2, Si, Si_3N_4 and Ge. Symmetry breaking at surfaces/interfaces can produce second-order nonlinearity, but its signal requires high-power excitation and is hard to be distinguished from the contribution of bulk multipole nonlinearity. Here, for the first time, we report second harmonic generation (SHG) originating deterministically from the surface nonlinearity of a silica microcavity. The bulk multipole nonlinear effects are eliminated via pumping a fundamental mode with transverse electric polarization, enabling the identification of surface nonlinear response. The doubly resonant enhancement of ultrahigh-Q cavity modes lowers the pump power below one milliwatt, and boosts the SHG conversion efficiency to 0.049% $\mathbf{W}^{-1}$, exceeding 10 orders of magnitude compared with the non-resonance case. This work can trigger intense applications in ultra-sensitive surface analysis, extend the frequency conversion range of silica photonic devices and possibly push the surface nonlinear effects into the quantum regime.

In materials with inversion symmetry, the second order nonlinearity originates from the asymmetric potential experienced by the surface layer and the bulk multipole response. The former source lies in the heart of the fruitful surface probe method, where the second harmonic and sum frequency generation are used to detect the surface properties, for example, the surface molecule arrangement and the adsorption or reaction of molecules on the surface. The metal surfaces or semiconductor surfaces with dangling bonds are preferable because of their enhanced or intrinsically large surface nonlinearity. Cavity-enhanced nonlinear optics with low pump power has seen dramatic development in the past decades with the demonstration of Raman laser, third harmonic emission, parametric oscillation and optical frequency combs. SHG in microcavities achieves extremely large conversion efficiency using materials with large second order susceptibility like $LiNbO_3$. The second order nonlinear signal in centrosymmetric material also benefits from the resonance enhancement in cavities. [fiber loop, SiN] A silica microsphere coated with nonlinear molecules can generate second harmonic with only a monolayer of surface coating. With a bare silica bottle resonator, the second harmonic signal was also observable at a continuous wave pump of 209 mW but the origin and properties of the SH remains unexplored. In addition to the enhancement, the ultrahigh Q presents a challenge on achieving phase-matching condition, which is known as the doubly resonant condition in a microcavity. Quasi-phase matching and dispersion engineering based on the geometry of cavity are common ways to realize phase matching, both of which, however, add to the complexity of the device fabrication and suffer from possible deviation from the design.

Here, second harmonic, originating from symmetry breaking at the surface and bulk multipole response (Fig. 1b), is observed under the continuous wave pump below 1 mW in a WGM microsphere made of centrosymmetric material. An unprecedented conversion efficiency of 0.049% W^{-1} benefits from doubly resonant enhancement of ultrahigh Q modes (phase-matching condition[also know as perfect phase matched]), which is achieved by thermal effect and optical Kerr effect. The work enriches the nonlinear toolbox of microcavity photonics and largely extends the emission range of silica microresonators with ultralow pump power, making it possible to push the frequency conversion process down to the quantum regime[refs in Asano OL]. More significantly, the fruitful surface SHG and SFG detection methods can be introduced into (bridged with?) the sensitive microcavity sensing, which enables surface-specific detection with low pump power and high sensitivity.

In the experiment, a silica microsphere (diameter ~ 62 μm) is pumped through a tapered optical fiber (waist diameter ~ 1 μm) at 1550 nm band [1, 2], as shown in Fig. 1a. To collect SH signal efficiently, a second fiber taper (waist diameter ~ 0.5 μm) designed for 780 nm band is incorporated into the system. The intrinsic quality factor (Q) for the pumped cavity mode is 4.8×10^7. Figure 1**c** shows a typical SH spectrum measured from the electron-multiplying CCD (EMCCD) and the corresponding pump spectrum measured from the optical spectrum analyzer (OSA). The SH signal appears at 777.75 nm when pumped at 1555.14 nm, which deviates only 0.023% from the expected wavelength, falling into the resolution tolerance of OSA and EMCCD. Note that stimulated Raman scattering and parametric oscillation do not occur because their thresholds are far above the pump power in the experiment. Third harmonic generation is also absent due to the phase mismatch in the nonlinear optical process. Moreover, SH signals arise in the full range when cavity modes are pumped from 1545 nm to 1565 nm, as shown in Fig. 1d. Among the occurrence

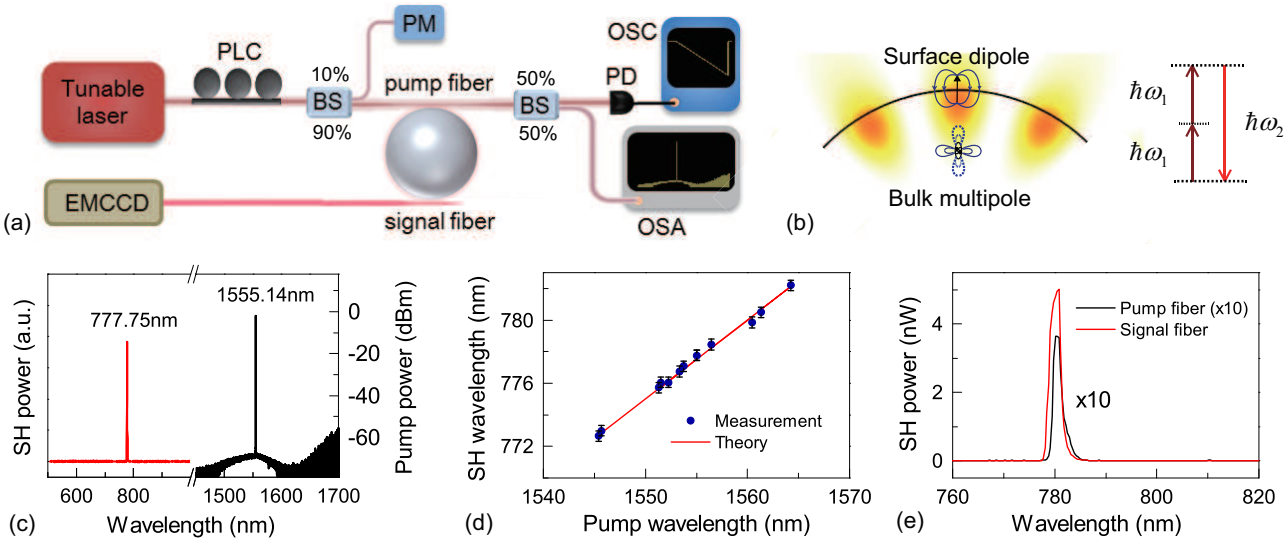

Figure 1: **Experimental set-up and observation of cavity-enhanced SH signals. a,** The pump light from a tunable laser around 1550 nm is coupled into a silica microsphere through a tapered fiber, and a second fiber is used to collect the SH signal. OSC: oscilloscope. OSA: optical spectrum analyzer. PLC: polarization controller. BS: beam splitter. EMCCD: electron-multiplying CCD. **b,** SH is generated from the surface dipole response and the bulk multipole response in a WG microsphere. **c,** Measured SH spectrum (red) and the corresponding pump spectrum (black). **d,** Measured SH wavelengths versus the corresponding pump wavelengths when different modes are pumped. **e,** Comparison of SH power collected by signal fiber and pump fiber (10 times magnified).

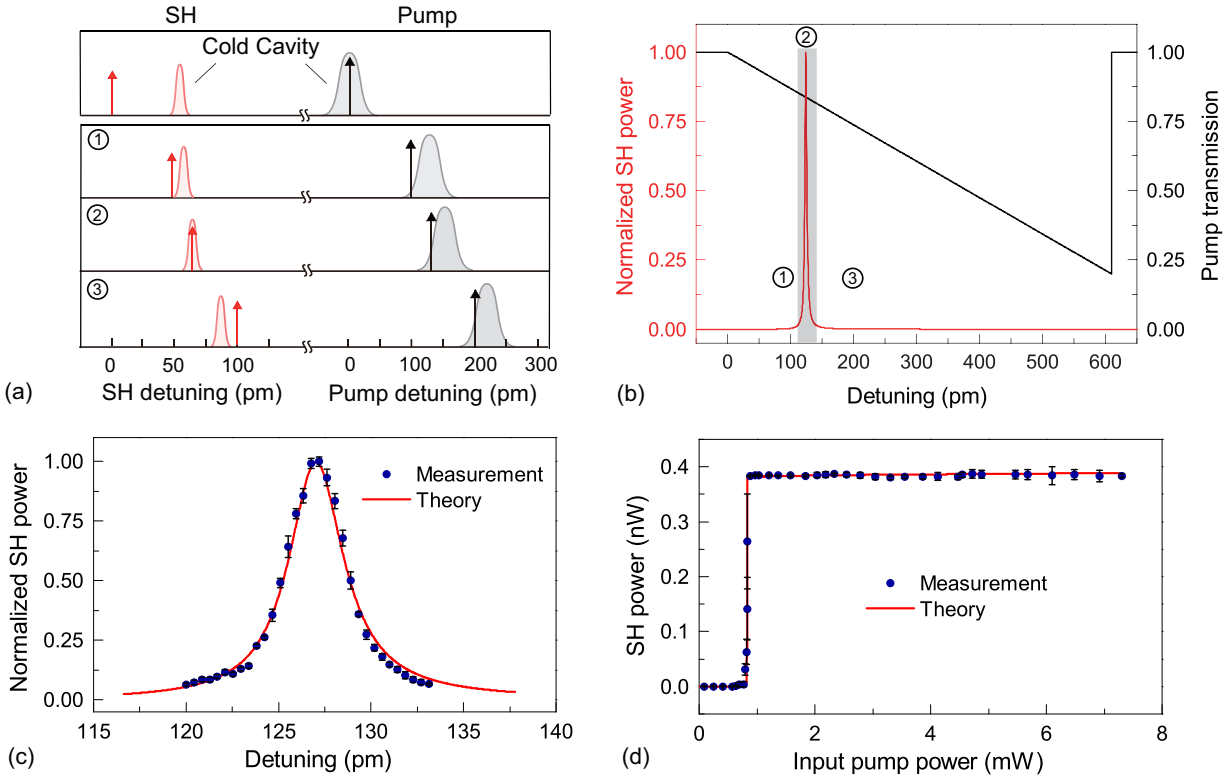

Figure 2: **Thermal effect and Kerr effect assisted phase-matching. a,** Schematic of the phase-matching process. Detuning here is the wavelength relative to the cold-cavity wavelength of the pumped mode (to half of this wavelength for SH detuning). The black (red) arrow represents the detuning of the pump light (its SH). The gray (red) Lorentzian line represents the pumped mode (SH mode). 1-3 show three states with increasing pump wavelength but the same input power. **b,** Normalized SH power and the pump transmission at different pump wavelength detuning. 1-3 correspond to the three states in panel **a**. The gray area is enlarged in panel **c** as the theoretical red line. **c,** SH power versus pump detuning with the input power of 4.46mW. **d,** The dependence of maximum SH power at all the pump detuning on the input power.

of SH, a maximum signal power of 5 nW was observed via the signal fiber. To compare the collecting efficiency of the two fibers, we optimize the fiber-cavity coupling so that the SH signal from the pump fiber is also observable, but the maximum signal power is still over one order of magnitude weaker than that from the signal fiber. From either fibers, SH signal is absent when the pump is off-resonance with cavity modes, which helps to eliminate the possibility of spurious signals such as the second order diffraction of the EMCCD grating.

The doubly resonant enhancement plays a pivotal role in efficient SHG, which is achieved by perfect phase-matching including momentum conservation and energy conservation. The former can be fulfilled by a pair of modes with proper angular momentum relation $m_2 = 2m_1$, where m_1 (m_2) is the angular number of the pump (SH) cavity mode. However, the material and geometric dispersion presents a challenge on energy conservation, obstructing the double resonance $\omega_2 = 2\omega_1$ and consequently, efficient SHG. More accurately, the SH power can be derived from coupled mode equations (see Supplementary Information)

$$P_2 = \frac{4|g|^2 Q_2^2/(\omega_2 Q_{1e})}{4Q_2^2(2\omega_p/\omega_2 - 1)^2 + 1} \frac{16Q_1^4 P_1^2/(\omega_1 Q_{2e})^2}{[4Q_1^2(\omega_p/\omega_1 - 1)^2 + 1]^2}, \tag{1}$$

where the subscripts 1, 2 represent the pumped mode and SH mode respectively, ω_i is the mode frequency and ω_p is the pump frequency, P_1 denotes the input pump power, g is the coupling coefficient between two modes, Q_i ($i = 1, 2$) stands for the loaded quality factor and Q_{ie} represents the external quality factor. The pump power depletion is ignored due to the weak second order nonlinear effect in silica. Equation (1) shows that ultrahigh Q is indispensable in boosting the SH power, while it also presents a challenge in double resonance by magnifying the frequency mismatch induced by the material and geometric dispersion. In order to compensate the dispersion, SH modes with higher order radial number was proposed or used [3][other], which relies on delicate geometric design of the cavity. In the experiment, however, the desired phase-matching can be disturbed by the deviation of cavity from its designed geometry, making one of the mode off-resonance and impeding highly efficient SHG. Therefore, to tune the cavity dispersion precisely and dynamically, we propose and experimentally realize a versatile method, leveraging mode frequency shift induced by thermal behavior (namely thermal expansion, thermally induced refractive index change and the optical Kerr effect) [4, 5].

The mechanism of thermal and Kerr assisted phase matching process is illustrated in Fig. 2a. When the pump power is weak and the mode frequency shift is negligible (cold cavity), the pumped (ω_{10}) and SH modes (ω_{20}) usually cannot be on resonance with the pump light and its SH simultaneously. With a larger input power, the pump mode experiences a red shift due to xxx: $\omega_1 = \omega_{10} - B_{11}|\alpha_1|^2$, where $|\alpha_1|^2$ is the intra-cavity power of the pumped mode and B_{11} is the coefficient of pump frequency shift. In this case, the wavelength of pump light should also increase to catch the pump mode, resulting in the non-Lorentzian, triangular transmission shape [carmon2004]. The SH mode also exhibits a red shift from the cold cavity frequency, which can be described by $\omega_2 = \omega_{20} - B_{12}|\alpha_1|^2$ where B_{12} is the coefficient of SH frequency shift. The thermal and Kerr effects of the SH are ignored in the analysis. In the process of tuning pump frequency from the cold cavity mode to resonance with the pump mode (state 1-3 in Fig. 2a), the larger rate of red shift for the SH of pump light ($\omega_p/2$) helps it to catch the SH mode (ω_2) at a certain pump-cavity detuning where the phase-matching condition is fulfilled the SH power reaches a peak value (state 2). Because of the ultrahigh Q of the SH resonance, the SH power diminishes rapidly before and after reaching the on-resonance frequency for SH (state 1 and 3 in Figs. 2a and b). xxx phase matching can also be realized in other cases with different rate of SH mode frequency shift or initial detuning between $\omega_p/2$ and ω_2 (see SI).

Using the phase matching method, we measure the SH power by tuning the pump frequency in the range of the gray area (Fig. 2b) with a fixed input power, as shown in Fig. 2c.Furthermore, the dependence of SH power on pump power is studied, as presented in Fig. 2d. Under each input power, we search for the maximum SH output power in the detuning range from the cold cavity mode to the on-resonance frequency for the pump. Among different values of input power, a critical power manifests itself, at which the SH of pump light achieves the resonance condition exactly when the pump becomes exactly resonant. In this case, the SH power is able to arrives at the peak value in Fig. 2c, which represents the most efficient SHG with the pump power of 879 μW and the conversion efficiency of 0.049% W^{-1}. Below the critical power, the SH of pump light is off resonance within the full detuning range, resulting in the extremely weak SH power. Above the critical power, the increasing input power at a fixed frequency pushes the pump mode farther to the red side (the pump is not completely on resonance) and consequently increases the detuning between the pump light and the cavity. The resulting reduced enhancement of the pump light counteracts with the increasing input power, leading to the almost steady intracavity power. [SI] The on-resonance frequency of the SH mode also remains unchanged with increasing input power, so that the intracavity power and consequently the SH power are almost unchanged as well.

Microresonator SHG in other materials usually use different phase matching strategy to achieve broadband phase matching, e.g. quasi-phase-matching [cite more later]. The quality factor is also moderate so that the thermal effect and Kerr effect do not manifest themselves in the SHG process. With xxx phase matching, it is also possible to obtain the explicit $P_2 \propto P_1^2$ dependence by introducing a degree of freedom other than the pump intracavity power to manipulate the SH mode frequency. For example, a control light or a heater can be incorporated into the system to change the intra-cavity power and thus achieving the double on-resonance condition at various input pump power. The specific measurement plan is beyond the scope of this [letter?].

In order to distinguish the contributions of surface and bulk nonlinearity, we investigate the polarization dependence, which originates from the nonlinear cou-

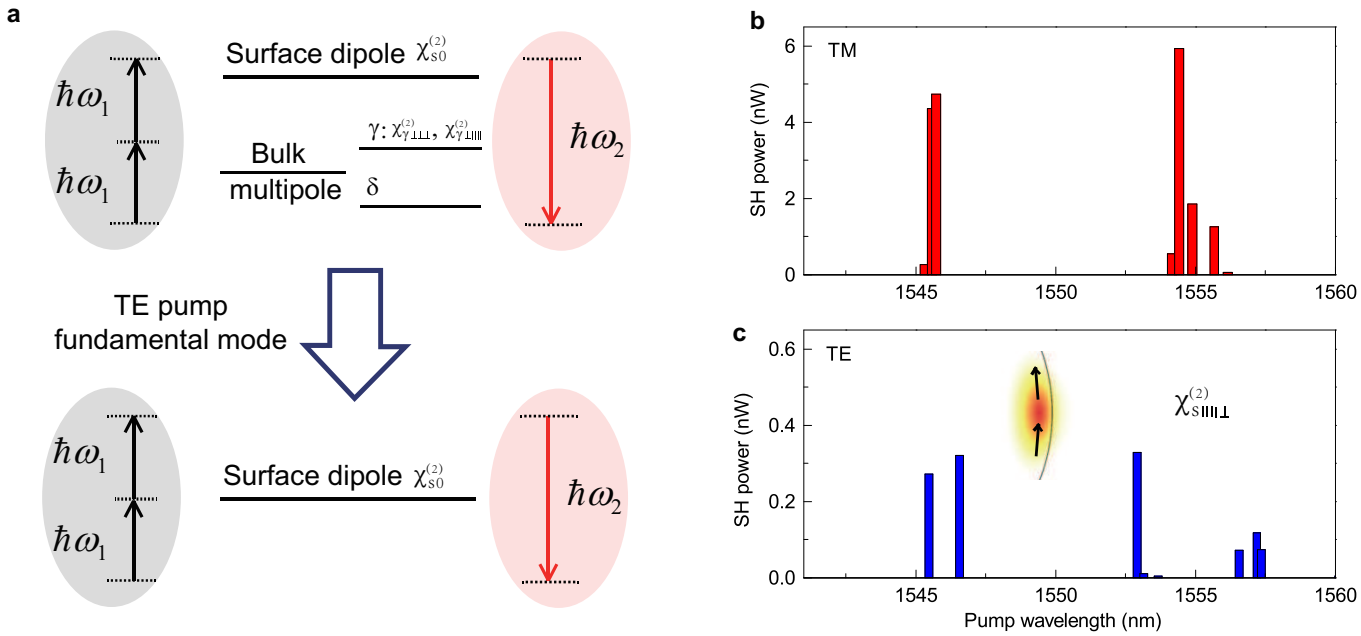

Figure 3: **Identification of surface nonlinearity from the bulk multipole response. a,** Origin of second order nonlinearity and the method to obtain surface-only nonlinear coupling. **b,c,** Measured second harmonic power at the corresponding pump wavelength with TM (**b**) and TE (**c**) pump polarization respectively. Inset in **c**: Field distribution of the target mode from numerical simulation(left) and measurement (right).

pling strength g in equation (1). The nonlinear coupling strength from surface dipole response can be written as

$$g_{s0} = 2\frac{\omega_1^2}{\omega_2 n^2}\frac{\int_{\text{surface}} \mathbf{E}_{02}^* : \chi_{s0}^{(2)} : \mathbf{E}_{01}\mathbf{E}_{01}\mathrm{d}\mathbf{S}}{\int |\mathbf{E}_{02}|^2 \mathrm{d}\mathbf{V}} \tag{2}$$

where n is the refractive index, $\chi_{s0}^{(2)}$ represents the surface nonlinear susceptibility, and $\mathbf{E}_{0i}(\mathbf{x})$ denotes the normalized electric field. The bulk multipole nonlinear polarization in silica can be expressed as $\mathbf{P}^{\text{bulk}} = \gamma\nabla(\mathbf{E}\cdot\mathbf{E}) + \delta(\mathbf{E}\cdot\nabla)\mathbf{E}$ [ref], where γ and δ are the nonlinear coefficients. The first term $\mathbf{P}_\gamma^{\text{bulk}}$ represents a longitudinal wave which can excite SH only at the surface. Therefore $\mathbf{P}_\gamma^{\text{bulk}}$ can contribute to an effective surface susceptibility $\chi_s^{(2)} = \chi_{s0}^{(2)} + \chi_{s,\gamma}^{(2)}$[6], corresponding to an effective coupling strength of g_s. The coupling strength induced by the second term $\mathbf{P}_\delta^{\text{bulk}}$ can be written as

$$g_b = 2\frac{\omega_1^2}{\omega_2 n^2}\frac{\delta\int \mathbf{E}_{02}^*\cdot(\mathbf{E}_{01}\cdot\nabla)\mathbf{E}_{01}\mathrm{d}\mathbf{V}}{\int |\mathbf{E}_{02}|^2\mathrm{d}\mathbf{V}} \tag{3}$$

Thus the total second order nonlinear coupling strength $g = g_s + g_b$, as shown in Fig. 3a.

The effective surface susceptibility tensor $\chi_s^{(2)}$ contains three non-zero components $\chi_{\perp\perp\perp}$, $\chi_{\parallel\parallel\perp}$ and $\chi_{\perp\parallel\parallel}$, where $\perp$ denotes the electric field direction perpendicular to the surface and $\parallel$ corresponds to the parallel direction. $\chi_{\perp\parallel\parallel}$ can be ignored in studying SHG due to the non-degeneracy of TM and TE pump modes. $\chi_{\perp\perp\perp}$ ($\chi_{\parallel\parallel\perp}$) plays a major role when TM (TE) mode is pumped, which only generates the TM polarized second harmonic in both cases. TM modes are preferable in surface induced SHG because $\chi_{\perp\perp\perp}$ is larger than $\chi_{\parallel\parallel\perp}$ [7]. Considering the bulk nonlinear response induced by $\mathbf{P}_\delta^{\text{bulk}}$, the coupling strength g_b relies on the specific field distribution in the cavity and the generated SH exhibits the same polarization as the pump mode. Note that for TE polarization, the field direction is along the polar direction, so that the polar symmetry of modes prohibits the excitation of SH modes with an even polar distribution from $\mathbf{P}_\delta^{\text{bulk}}$. While the TM pump modes, with electric field along the radial direction, can excite second harmonic without the above restriction. Because of a stronger confinement in the radial direction than the polar direction and thus a larger divergence for most of the modes, TM modes tend to link with a larger g_b than TE modes. Consequently, from both the surface and the bulk second order nonlinearity, TM pump modes can generate stronger SH signals statistically In the experiment, transverse magnetic (TM) or transverse electric (TE) modes from 1545 nm to 1565 nm are pumped separately by adjusting the polarization of the pump light. The TM pump modes exhibit larger SH power, as shown in Fig. 3b and c, which agrees with the theoretical analysis.

The polarization dependence can be utilized to identify the surface nonlinearity from the bulk nonlinear response of both $\mathbf{P}_\gamma^{\text{bulk}}$ and $\mathbf{P}_\delta^{\text{bulk}}$. The former effect does not contribute to susceptibility $\chi_{\parallel\parallel\perp}$, corresponding to the TE polarized pump [heinz]. The latter can also be discerned from the surface nonlinear response with the TE polarized pump. In this case, an SH signal with a TM polarization can only originate from the surface nonlinearity ($\chi_{\parallel\parallel\perp}$) because $\mathbf{P}_\delta^{\text{bulk}}$ requires the same polarization between the pump mode and the SH mode. Furthermore, when a fundamental [] TE mode (angular number $l_1 = m_1$) is pumped, only the fundamental SH modes (angular number$l_2 = m_2$) are allowed by the selection rule [], which cannot be excited from $\mathbf{P}_\delta^{\text{bulk}}$ due to even polar field distribution of the SH mode. In the measurement, a surface-only second harmonic is obtained determinis-

tically by employ a fundamental TE pump mode at xx nm without measuring the SH polarization, as shown in the left inset in Fig. 3c. Here the fundamental TE pump mode is confirmed experimentally by measuring the transmission while scanning the relative angular position of the pump fiber and the cavity, as illustrated in the Fig. 3c.

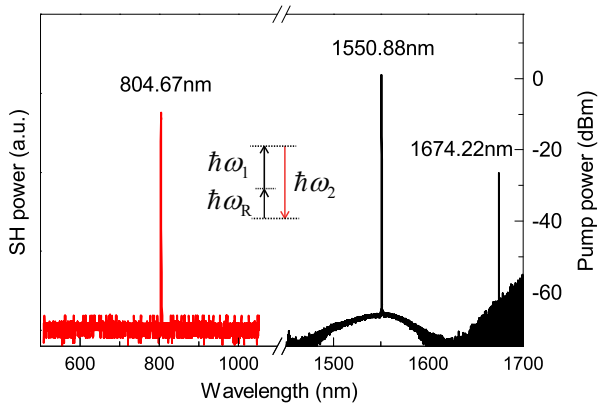

Figure 4: **Measured spectra of second-order sum frequency generation (SFG).** The pump light (ω_1) and Raman light (ω_2) are summed to generate the SF signal (ω_3).

Additionally, sum frequency generation (SFG) can also arise when a Raman signal is stimulated by the pump light. Shown in Fig. 4 is an SF signal (804.67 nm) and the corresponding pump (1550.88 nm) and its Raman signal (1674.22 nm) with an input power of 7.33 mW, which is above the Raman threshold for this mode. The deviation of the SF wavelength from the expected value (804.63 nm) is much smaller than the resolution of EMCCD.

[Conclusion]

References

[1] J Cheung Knight, G Cheung, F Jacques, and TA Birks. Phase-matched excitation of whispering-gallery-mode resonances by a fiber taper. *Optics letters*, 22(15):1129–1131, 1997.

[2] Ming Cai, Oskar Painter, and Kerry J Vahala. Observation of critical coupling in a fiber taper to a silica-microsphere whispering-gallery mode system. *Physical review letters*, 85(1):74, 2000.

[3] Gregory Kozyreff, JL Dominguez Juarez, and Jordi Martorell. Whispering-gallery-mode phase matching for surface second-order nonlinear optical processes in spherical microresonators. *Physical Review A*, 77(4):043817, 2008.

[4] Pascal DelHaye, T Herr, E Gavartin, ML Gorodetsky, Ronald Holzwarth, and Tobias J Kippenberg. Octave spanning tunable frequency comb from a microresonator. *Physical Review Letters*, 107(6):063901, 2011.

[5] T Herr, V Brasch, JD Jost, CY Wang, NM Kondratiev, ML Gorodetsky, and TJ Kippenberg. Temporal solitons in optical microresonators. *Nature Photonics*, 8(2):145–152, 2014.

[6] Tony F Heinz. Second-order nonlinear optical effects at surfaces and interfaces. *Nonlinear surface electromagnetic phenomena*, 29, 1991.

[7] Francisco J Rodriguez, Fu Xiang Wang, and Martti Kauranen. Calibration of the second-order nonlinear optical susceptibility of surface and bulk of glass. *Optics express*, 16(12):8704–8710, 2008.